Effect of metal oxide arrester on the chaotic oscillations in the voltage transformer with nonlinear core loss model using chaos theory

Hamid Reza Abbasi[a)†], Ahmad Gholami[a)], Seyyed Hamid Fathi[b)], and Ataollah Abbasi[b)]

[a)] *Iran University of Science & Technology, Electrical & Electronic Engineering Department, Narmak* 1684613144, *Tehran, Iran*
[b)] *Amirkabir University, Electrical Engineering Department, Tehran* 64540, *Iran*

(Received 19 March 2013; revised manuscript received 14 June 2013; published 19 November 2013)

In this paper, controlling chaos when chaotic ferroresonant oscillations occur in a voltage transformer with nonlinear core loss model is performed. The effect of a parallel metal oxide surge arrester on the ferroresonance oscillations of voltage transformers is studied. The metal oxide arrester (MOA) is found to be effective in reducing ferroresonance chaotic oscillations. Also the multiple scales method is used to analyze the chaotic behavior and different types of fixed points in ferroresonance of voltage transformers considering core loss. This phenomenon has nonlinear chaotic dynamics and includes sub-harmonic, quasi-periodic, and also chaotic oscillations. In this paper, the chaotic behavior and various ferroresonant oscillation modes of the voltage transformer is studied. This phenomenon consists of different types of bifurcations such as period doubling bifurcation (PDB), saddle node bifurcation (SNB), Hopf bifurcation (HB), and chaos. The dynamic analysis of ferroresonant circuit is based on bifurcation theory. The bifurcation and phase plane diagrams are illustrated using a continuous method and linear and nonlinear models of core loss. To analyze ferroresonance phenomenon, the Lyapunov exponents are calculated via the multiple scales method to obtain Feigenbaum numbers. The bifurcation diagrams illustrate the variation of the control parameter. Therefore, the chaos is created and increased in the system.

Keywords: ferroresonance, chaos theory, metal oxide arrester, Lyapunov exponent

PACS: 82.40.Bj, 95.10.Fh, 75.60.Ej, 05.45.–a **DOI:** 10.1088/1674-1056/23/1/018201

1. Introduction

The ferroresonance is a complex nonlinear phenomenon, which may cause thermal and insulation problems in transmission and distribution systems.[1–3] Due to nonlinear nature of ferroresonance, linear methods cannot be used. Thus, the investigation of this behavior is possible by employing more complex numerical methods[4,5] and programs such as Matlab, electro magnetic transient program (EMTP), and power system computer aided design (PSCAD).[6–10] The ferroresonance circuits consist of a linear capacitance and a nonlinear inductance and can lead to overvoltages, overcurrents, and chaos in a power system in wide frequency range. The core of voltage transformer is presented by a nonlinear inductance. The capacitances of system are considered as a linear capacitance. These capacitances are line-to-line, line-to-ground, and circuit breakers grounding capacitances. Due to nonlinear nature of circuit elements, the number of fixed points is more than one. Thus, the variation of system parameters leads to instability of fixed points. This behavior depends on the frequency and electrical source amplitude, initial conditions, and core loss.[11–13] Although methods such as harmonic balance can be used to analyze nonlinear differential equations, solving them leads to a set of complex algebraic equations.[14] Most of ferroresonance studies have relatively high computational processes and their application is so limited for practical cases. An alternative solution is the bifurcation theory which has been implemented in Refs. [15]–[20]. This method has the potential to describe and analyze qualitative characteristics of solutions, i.e., fixed points, as the system parameters change. In addition, creating a bifurcation diagram with a continuous method can be more systematic, with reduced computational operations.[14] The ferroresonance has been analyzed using bifurcation theory in Refs. [3] and [21]–[24]. The chaotic ferroresonant behavior depends on several system parameters such as: source voltage amplitude, capacitance, resistance, core loss, and initial conditions.[8,17,21,25,26] Also, metal oxide arrester (MOA) and neutral resistance lead to damping and even elimination of chaotic oscillations. The chaotic behavior can be changed when MOAs are connected to the transformer terminals.[22,24–28] The ferroresonance has a wide frequency spectrum with subharmonics, interharmonics, and harmonics. In Ref. [7], only subharmonic resonances have been considered and a linear resistance has been used to model the transformer core loss. To increase system stability, the ferroresonance in the voltage transformer should be detected and damped; otherwise, protection relays would remove it from the power system. After detecting this condition, one can use thyristor-based limiter to lower its effects.

In the present paper, a linear and two nonlinear models are considered for the transformer core loss. The bifurcation

†Corresponding author. E-mail: habbasi@iust.ac.ir

© 2014 Chinese Physical Society and IOP Publishing Ltd

diagrams, phase planes,[29–32] Feigenbaum numbers, and Lyapunov exponents are used to analyze the chaos route to ferroresonant behavior of voltage transformers. The Lyapunov exponents and the routes to chaos are analyzed using multiple scales method and bifurcation theory, respectively. The multiple scales method is used to calculate eigenvalues regularly. If any changes in eigenvalues result in bifurcation in the system, it is possible to detect its type and observe the system behavior according to the logic of chaotic behavior. In this work, effect of core loss nonlinear models using bifurcation diagram is illustrated. The MOA is used in the system concerned, and its effect on clamping ferroresonant over voltage is analyzed. In addition, the effect of the core nonlinearity is studied using the bifurcation diagram. The stability is analyzed using Lyapunov exponents and bifurcation diagrams. Furthermore, in the bifurcation diagrams, stable and unstable solutions and type of the bifurcation are also specified in bifurcation diagrams. Finally, the stability of periodic solutions is determined using solution characteristics.

2. System modeling

The single line diagram of the studied system is shown in Fig. 1. In this system, the capacitances C_{sh1} and C_{sh2} present the proximity effect of reserve and main buses. The capacitances C_s are parallel capacitances with coupling circuit breakers. The parameters in this paper are defined in Table 1. The voltage transformer is connected to the reserve busbar for voltage measurement.

When voltage is induced in the reserve bus and disconnectors, both sides of circuit breaker are opened and the circuit breaker is closed, so the electromagnetic force needed for ferroresonance is generated. Grounding capacitors and capacitors between the main and reserve buses cause the induced voltage increase to its nominal value. When the disconnectors are closed, the capacitors are connected to the lower voltage bus, i.e., the main bus and also the reserve bus. Due to low thermal capacity of voltage transformers, ferroresonance would damage their insulation severely.

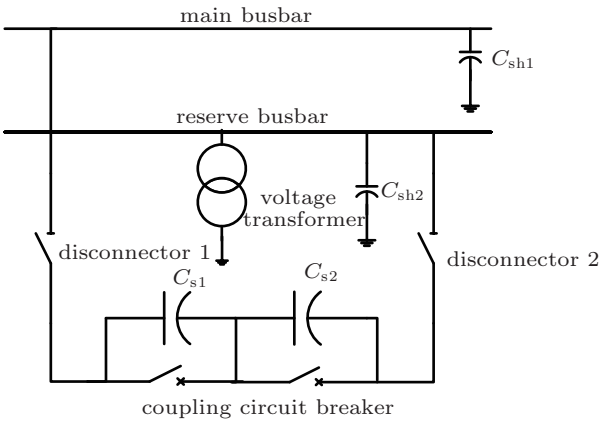


Fig. 1. Single line diagram of the studied system.

Table 1. Definition of the parameters in this paper.

Parameter	Definition	Parameter	Definition
h_i	coefficient of core loss nonlinear function	ε	small positive parameter
a	coefficient of linear part of magnetizing curve	μ	damping coefficient
b	coefficient of nonlinear part of magnetizing curve	$K\varepsilon$	amplitude of voltage source
ω	angular frequency of voltage source	δ	external detuning
q	index of nonlinearity of the magnetizing curve	λ	eigenvalue
C_{ser}	series linear capacitor	M	mondoromy matrix
C_{sh}	shunt linear capacitor	$\psi(t)$	fundamental matrix
x	state variable	i_R	loss current of core
$i(t)$	instantaneous value of branch current	V_m	magnetization voltage
$v(t)$	instantaneous value of voltage	R_{min}	minimum resistance of circuit
ϕ	flux linkage of the nonlinear inductance	ϕ_{rated}	nominal flux
R_{max}	maximum resistance of circuit	σ	constant greater than 1
χ	Feigenbaum constant		

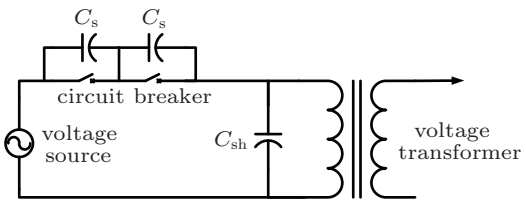


Fig. 2. Equivalent circuit of Fig. 1.

The equivalent circuit of Fig. 1 is shown in Fig. 2. The grading capacitors are in series. Capacitors between the main and reserve buses and also buses and ground are modeled with a capacitor in parallel with the voltage transformer.

The amplitude of the voltage source is equal to voltage of the main bus. The core of voltage transformer is modeled by a nonlinear inductance and a resistance representing core losses. The voltage transformer core is an important factor in investigating the ferroresonance.[11] The base values of the case study in this paper are $275/\sqrt{3}$ kV, 100 kVA, and 50 Hz. The magnetization curve of the transformer is modeled with a

polynomial function in the form of

$$i_1 = a\phi + b\phi^q. \tag{1}$$

The term $a\phi$ models the linear behavior and $b\phi^q$ represents the saturation effect of the core. The coefficients used in Eq. (1) are defined as follows: for $q = 7$, $a = 3.42$ and $b = 0.41$; for $q = 11$, $a = 3.42$ and $b = 0.14$.

The dynamics of the equivalent circuit can be described by the following nonlinear differential equation:

$$\frac{\mathrm{d}^2\phi}{\mathrm{d}t^2} + \frac{1}{R(C_{\mathrm{sh}}+C_{\mathrm{ser}})}\frac{\mathrm{d}\phi}{\mathrm{d}t} + \frac{1}{(C_{\mathrm{sh}}+C_{\mathrm{ser}})}(a\phi + b\phi^q) = \frac{C_{\mathrm{ser}}\omega}{(C_{\mathrm{sh}}+C_{\mathrm{ser}})}\left(\sqrt{2}V_{\mathrm{rms}}\cos(\omega t)\right), \tag{2}$$

where X_1, X_2, ε, μ, and k are defined as follows:

$$X_1 = \phi, \tag{3}$$

$$X_2 = V, \tag{4}$$

$$\varepsilon = \frac{1}{(C_{\mathrm{sh}}+C_{\mathrm{ser}})}, \tag{5}$$

$$\mu = \frac{1}{R}, \tag{6}$$

$$K = C_{\mathrm{ser}}\omega(\sqrt{2}V_{\mathrm{rms}}). \tag{7}$$

Substituting X_1, ε, μ, and k into Eq. (2), the following equation is obtained:

$$\ddot{X}_1 + \varepsilon\mu(aX_1 + bX_1^q) = K\varepsilon\cos(\omega t). \tag{8}$$

The state space representations are given by

$$\dot{X} = AX + BU, \tag{9}$$

where

$$\dot{X}_1 = X_2, \tag{10}$$

$$\dot{X}_2 = -\varepsilon\mu(aX_1 + bX_1^q) - \varepsilon\mu X_2 + K\varepsilon\cos\theta. \tag{11}$$

Then, we have

$$\dot{\boldsymbol{X}} = \begin{bmatrix}\dot{X}_1\\ \dot{X}_2\end{bmatrix} = \begin{bmatrix}0 & 1\\ -a\varepsilon & -\varepsilon\mu\end{bmatrix}\begin{bmatrix}X_1\\ X_2\end{bmatrix} + \begin{bmatrix}0 & 0\\ -b\varepsilon & 0\end{bmatrix}\begin{bmatrix}X_1^q\\ 0\end{bmatrix} + \begin{bmatrix}0\\ K\varepsilon\end{bmatrix}U(t), \tag{12}$$

where $U(t) = \cos\omega t$.

The fixed or equilibrium points are defined as the zero crossing points of the vector field,

$$\dot{X} = 0. \tag{13}$$

At equilibrium points, the right-hand side of Eq. (9) becomes zero. Then, the stability of this equation is dominated by the eigenvalues of the Jacobian calculated at the fixed point.

3. Multiple scales method

This method can be used for stability and bifurcation analysis.[33] Using this method, the first-order approximation can be obtained for the solution of Eq. (8) as follows:

$$X_1 = h\cos(\omega t - \gamma) + O(\varepsilon). \tag{14}$$

The parameters μ, a, and k are independent of ε. Moreover, the frequency of the system is

$$\omega = 1 + \varepsilon\delta. \tag{15}$$

Using this method, the first-order uniform expansion of Eq. (11) is of the form

$$X_1(t;\varepsilon) = X_{1,0}(T_0, T_1) + \varepsilon X_{1,1}(T_0, T_1) + \cdots, \tag{16}$$

where $T_0 = t$ and $T_1 = \varepsilon T_0$.

The time derivative, in terms of T_1, is given by

$$\frac{\mathrm{d}}{\mathrm{d}t} = D_0 + \varepsilon D_1 + \varepsilon^2 D_2 + \cdots \tag{17}$$

Substituting Eqs. (16) and (17) into Eq. (8) yields

$$O(\varepsilon^0): \quad D_0^2 X_{1,0} = 0, \tag{18}$$

$$O(\varepsilon): \quad D_0^2 X_{1,1} + 2D_1 D_0 X_{1,0} + \mu D_0 X_{1,0} + bX_{1,1}^q = K\cos\omega_0 t. \tag{19}$$

The solution of Eq. (18) can be expressed as follows:

$$X_{1,0} = A(T_1)T_0 + A_0. \tag{20}$$

Substituting Eq. (18) into Eq. (19) yields

$$D_0^2 X_{1,1} + aX_{1,1} + bX_{1,1}^q = -2A' - \mu A + \frac{K}{2}\mathrm{e}^{\mathrm{i}5T_1} + \mathrm{cc}, \tag{21}$$

where cc denotes a complex conjugation of the preceding terms and the prime denotes the derivation with respect to T_1. Using Eq. (8), the secular terms of $X_{1,1}$ can be obtained as

$$2A' - \mu A + \frac{K}{2}\mathrm{e}^{\mathrm{i}5T_1} = 0. \tag{22}$$

Considering A in a polar form ($A = \frac{1}{2}\alpha\exp[\mathrm{i}(\beta + \delta T_2)]$, α and β are functions of T_1) and separating real and imaginary parts of Eq. (19), we obtain

$$\alpha\beta' + \alpha\delta + \frac{K}{2}\sin\beta = 0, \tag{23}$$

$$\frac{1}{2}\alpha'\alpha - \frac{K}{2}\cos\beta = 0. \tag{24}$$

Setting $\alpha' = 0$ and $\beta' = 0$, the fixed points are expressed by

$$\alpha_0\delta + \frac{K}{2}\sin\beta_0 = 0, \tag{25}$$

$$\frac{1}{2}\alpha_0 - \frac{K}{2}\cos\beta_0 = 0. \tag{26}$$

Manipulating Eqs. (25) and (26) leads to

$$\alpha_0^2\delta^2+\frac{1}{4}\alpha_0^2=\frac{1}{4}K^2. \tag{27}$$

The stability of fixed points depends on eigenvalues of the following Jacobian matrix:

$$\boldsymbol{A}=\begin{bmatrix}\frac{1}{2} & \frac{K}{2}\sin\beta\\ \frac{K}{2\alpha^2}\sin\beta & -\frac{K}{2}\cos\beta\end{bmatrix}. \tag{28}$$

The eigenvalues can be determined by solving the following equation:

$$\lambda^2+\left(\frac{K}{2\alpha}\cos\beta\right)\lambda-\frac{K}{4\alpha}\cos\beta-\frac{K^2}{4\alpha^2}\sin^2\beta=0. \tag{29}$$

Substituting the polar form of $\boldsymbol{A}$ into Eq. (8) using the result of Eq. (18), the first approximation X_1 can be written as

$$X_1=\alpha\cos(\omega t+\beta)+\cdots. \tag{30}$$

If $k=0$, then we have

$$\begin{cases}\alpha\beta=-\alpha\delta,\\ \alpha'=-\frac{1}{2}\alpha.\end{cases} \tag{31}$$

Neglecting simple answers, $\alpha\neq 0$, it is obvious that if $T_1=\varepsilon t$,

$$\beta=-\varepsilon\delta t+\beta_0. \tag{32}$$

Therefore, the free oscillations of Eq. (8) can be presented by the following equation up to the first-order approximation:

$$X_1=a\cos(\omega_0 t+\beta_0)+\cdots. \tag{33}$$

The equation of eigenvalues leads to

$$\lambda^2+\left(\frac{1}{2}\alpha_0-\frac{1}{2}\right)\lambda-\frac{1}{4}-\delta^2=0. \tag{34}$$

In this section, the first-order approximation of Eq. (8) is obtained using the multiple scales method and the stability analysis is analyzed using the chaos theory. By using this method, the eigenvalues are calculated for each bifurcation. As a result, the type of the bifurcation can be determined in bifurcation diagrams.

4. Simulation results

In this section, the core loss model is in the form of the following polynomial function:[34]

$$i_{\mathrm{R}}=h_0+h_1V_{\mathrm{m}}+h_2V_{\mathrm{m}}^2+h_3V_{\mathrm{m}}^3. \tag{35}$$

The dynamics of the system is expressed by

$$\frac{\mathrm{d}^2\lambda}{\mathrm{d}t^2}+\frac{1}{(C_{\mathrm{sh}}+C_{\mathrm{ser}})}\left(h_1\frac{\mathrm{d}\lambda}{\mathrm{d}t}+\left(h_2\frac{\mathrm{d}\lambda}{\mathrm{d}t}\right)^2+\left(h_3\frac{\mathrm{d}\lambda}{\mathrm{d}t}\right)^3\right)\times\frac{1}{(C_{\mathrm{sh}}+C_{\mathrm{ser}})}(a\lambda+b\lambda^q)+\frac{h_0}{(C_{\mathrm{sh}}+C_{\mathrm{ser}})}=\frac{C_{\mathrm{ser}}\omega}{(C_{\mathrm{sh}}+C_{\mathrm{ser}})}\left(\sqrt{2}V_{\mathrm{rms}}\cos(\omega t)\right). \tag{36}$$

For the studied voltage transformer, the coefficients h_0, h_1, h_2, and h_3 are[34] $h_0=-0.00067$, $h_1=3.1543$, $h_2=-4.89933$, and $h_3=2.61744$. As V_{in} increases, the system enters the saturation section of the magnetization curve and the ferroresonance occurs. In Figs. 3 and 4, this phenomenon can be observed. Although the behavior of the system shows that there is a single frequency, the PDB occurs. The magnetization curve and the voltage waveform for $V_{\mathrm{in}}=3.5$ pu and $q=7$ are shown in Figs. 3 and 4, respectively. The voltage waveform reveals single frequency of the system behavior, but shows that the system behavior has an undesirable effect on the system insulation and could damage it.

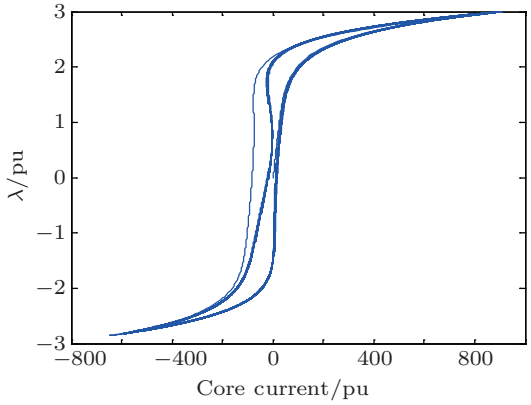


Fig. 3. (color online) Nonlinear transformer magnetization curve for the second nonlinear model for $V_{\mathrm{in}}=3.5$ pu and $q=7$.

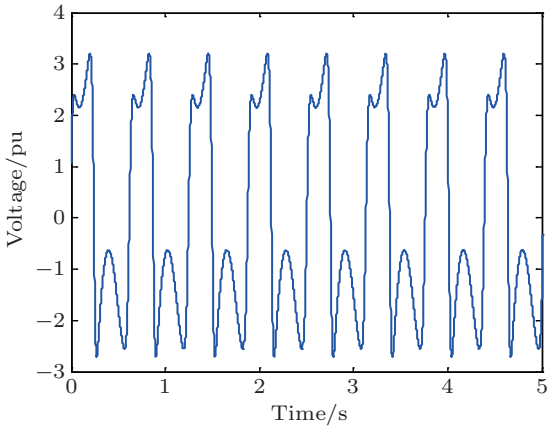


Fig. 4. (color online) Voltage waveform for $V_{\mathrm{in}}=3.5$ pu and $q=7$.

For comparison, the bifurcation diagrams for $q=7$ and 11 are shown in Figs. 5 and 6. This nonlinear core loss model shows the hysteresis effect better than the previous models. Also, bifurcation diagram of this model also exhibits the dynamic behavior of the ferroresonance more clearly. Using this

bifurcation diagram, one can analyze the complexity of trajectories. The blue route has the main frequency of the voltage source. Before the limit of $V_{\rm in} = 0.83$ pu, the voltage is stable with a frequency of 50 Hz. Then, at point (1), the voltage in the terminal of transformer increases to 2.2 pu.

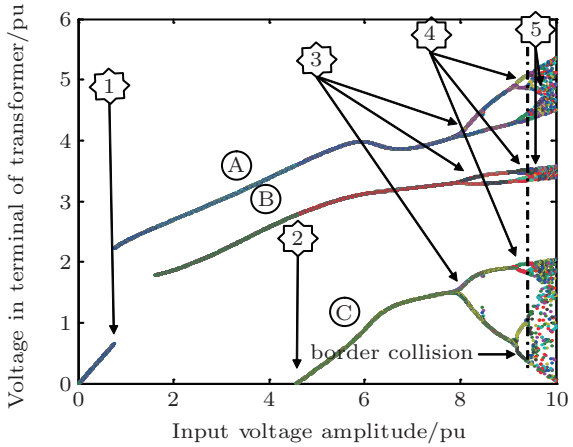


Fig. 5. (color online) Bifurcation diagram for the second nonlinear model for $q = 7$.

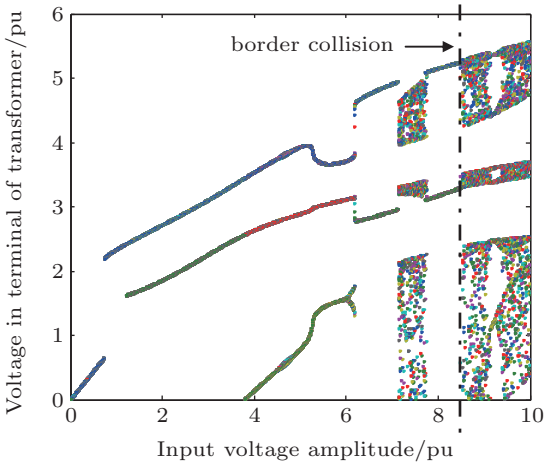


Fig. 6. (color online) Bifurcation diagram for the second nonlinear model for $q = 11$.

The fixed points are stable and the output voltage is single-frequency. This behaviour continues from $V_{\rm in} = 0.83$ pu to $V_{\rm in} = 1.57$ pu. At $V_{\rm in} = 1.57$ pu, another path emerges in the output voltage, which continues from path (B) (green path). With further increase in $V_{\rm in}$, the other frequency emerges in the output voltage at $V_{\rm in} = 4.62$ pu (path C). At $V_{\rm in} = 7.98$ pu, i.e., points (3-A), (3-B), and (3-C), the PDB$^{(1)}$ occurs in each path. This behavior continues until points (4-A), (4-B), and (4-C), where PDB$^{(2)}$ occurs in each path. This process continues until the system enters into chaotic regions at points (5-A), (5-B), and (5-C). The border collision bifurcation is shown in Fig. 5. The main reason for this collision is a crisis.

Crises are collisions between a chaotic attractor and a coexisting unstable fixed point or periodic orbit (or its stable manifold). In this situation, the attractor seems to expand suddenly.[35] This happens when the unstable period-2 fixed point touches the chaotic attractor. These unstable (fixed) equilibrium points repel the trajectory out of the sub-bands in such a way that the regions between the bands are also filled chaotically, resulting in an expansion of the attractor. This is called an interior crisis. As the crisis point is approached, transient chaos could be found and the system becomes chaotic, which can be from the interior crisis or emerging type.

At an interior crisis of emerging type, due to the collision with an n-periodic flip saddle, the $2n$ pieces of a chaotic region merge two by two, giving rise to an n-piece chaotic attractor. As shown in the bifurcation diagram, when the nonlinear model of the transformer core loss is considered, the chaos occurrence is postponed. The reason for this delay can be investigated by obtaining the system dynamic equation for both linear and nonlinear cases. It reveals the impact of 2nd- and 3rd-order damping parts on the dynamics of the nonlinear case in high and low amplitude harmonic resonances, eliminating their effects on the system behavior. Table 2 shows eigenvalues for PDB$^{(1)}$ and PDB$^{(2)}$. These eigenvalues are obtained by the multiple scales method.

Table 2. Eigenvalues for PDBs.

PDB$^{(i)}$	Path		
	A	B	C
PDB$^{(1)}$	–2.32, –0.81	–3.19, –0.723	–1.84, –0.65
PDB$^{(2)}$	–1.76, –0.46	–2.11, –0.134	–1.46, –0.31

The bifurcation diagram shown in Fig. 6 is for $q = 11$. Equation (1) is rewritten as

$$i_{\rm L} = 3.42\phi + 0.014\phi^{11}. \tag{37}$$

The border collision bifurcation is shown in Fig. 6. As mentioned, the chaos is due to interior crisis in this situation.

This bifurcation diagram is similar to the previous one shown in Fig. 5. However, this figure cannot exhibit the nonlinearity and complexity of the system clearly. The sequence of bifurcation parameters obeys a geometric law with Feigenbaum constant.[36] This constant is obtained by using the following limit:

$$\chi = \lim_{i\to\infty}\left\{\frac{a_i - a_{i-1}}{a_{i+1} - a_i}\right\} \approx 4.6692016. \tag{38}$$

For practical applications, mentioned limit cannot be easily determined. Therefore, an estimation of the Feigenbaum constant can be obtained from a finite sequence. In path A: PDB$^{(1)}$: $a_1 = 1.7831$, PDB$^{(2)}$: $a_2 = 8.001$, PDB$^{(3)}$: $a_3 = 9.3326$, and

$$\chi = \lim_{i\to\infty}\left\{\frac{8.001 - 1.7931}{9.3326 - 8.001}\right\} \approx 4.6694. \tag{39}$$

Chaos occurrence delay is due to the damping term in core loss function. However, it can be observed that by increasing

q, the chaos occurs in lower values of $V_{\rm in}$. The nonlinear core loss model mitigates the chaotic ferroresonance behavior in the voltage transformer. In addition, the presence of the nonlinear term in dynamic equations of core loss function results in more regular PDBs.

5. Effect of metal oxide arrester on the chaotic ferroresonant oscillations

The base system model adopted from Ref. [14] with the MOA arrester connected across the voltage transformer winding is shown in Fig. 7. Linear approximation of the peak current of the magnetization reactance can be given by

$$i_1 = a\phi. \tag{40}$$

However, for very high currents, the iron core might be saturated where the flux-current characteristic becomes highly nonlinear. Arrester can be expressed by

$$V = KI^{\alpha}, \tag{41}$$

where V represents the resistive voltage drop, I represents the arrester current, K is constant, and α is the nonlinearity constant. The differential equation for the circuit in Fig. 7 can be written as

$$\begin{aligned}&\frac{{\rm d}^2\phi}{{\rm d}t^2}+\frac{1}{C_{\rm ser}+C_{\rm sh}}\left(h_1\frac{{\rm d}\phi}{{\rm d}t}+\left(h_2\frac{{\rm d}\phi}{{\rm d}t}\right)^2+\left(h_3\frac{{\rm d}\phi}{{\rm d}t}\right)^3\right.\\&\left.+\left(\frac{({\rm d}\phi/{\rm d}t)}{k}\right)^{\alpha}{\rm sign}\left(\frac{{\rm d}\phi}{{\rm d}t}\right)\right)\\&+\left(\frac{1}{C_{\rm ser}+C_{\rm sh}}\right)(a\phi+b\phi^q)+\frac{h_0}{C_{\rm ser}+C_{\rm sh}}\\&=\left(\frac{C_{\rm ser}\omega}{C_{\rm ser}+C_{\rm sh}}\right)\cos\omega t.\end{aligned} \tag{42}$$

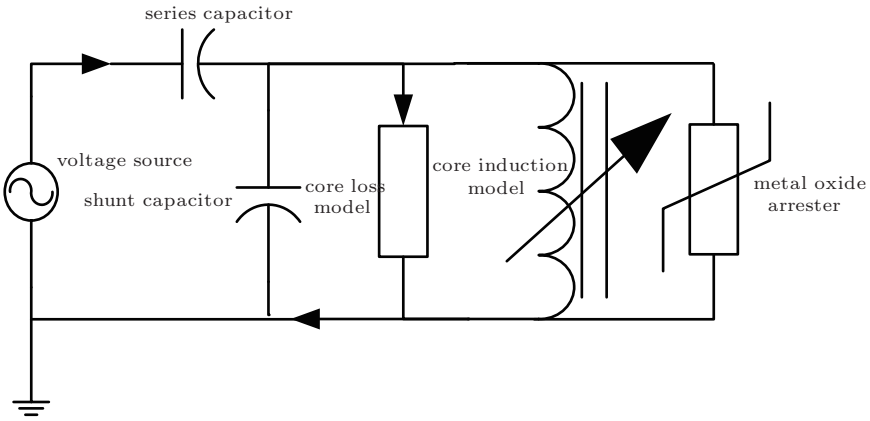


Fig. 7. Base system model with the MOA arrester connected across the voltage transformer winding.

Table 3. Behavior of system without MOA for $V_{\rm in} = 0.5$, 1, 2, 3, 4, and 5 pu.

E	0.5	1	2	3	4	5
q= 7	sin	sin	PDB	HB	chaotic	chaotic
q = 11	sin	sin	PDB	chaotic	chaotic	chaotic

Table 4. Behavior of system with MOA for $V_{\rm in} = 0.5$, 1, 2, 3, 4, and 5 pu and $\alpha = 25$.

E	0.5	1	2	3	4	5
q = 7	sin	sin	sin	PDB	PDB	PDB
q = 11	sin	sin	sin	PDB	HB	chaotic

Using the multiple scales method, Tables 3–6 are given for different values of $V_{\rm in}$, to analyze the circuit with and without MOA. Table 3 shows behavior of system for $V_{\rm in} = 0.5$, 1, 2, 3, 4, 5 pu and $q = 7$, 11 without MOA. Table 4 shows behavior of system with MOA when $\alpha = 25$. Table 5 shows behavior of system with MOA when $\alpha = 27$, and Table 6 is for $\alpha = 31$. It is found from Tables 3–6 that by increasing α chaotic oscillation is eliminated and the behavior of system can be stabilized.

Table 5. Behavior of system with MOA for $V_{\rm in} = 0.5$, 1, 2, 3, 4, 5 pu and $\alpha = 27$.

E	0.5	1	2	3	4	5
q= 7	sin	sin	sin	sin	PDB	PDB
q = 11	sin	sin	sin	PDB	PDB	chaotic

Table 6. Behavior of system with MOA for $V_{\rm in} = 0.5$, 1, 2, 3, 4, 5 pu and $\alpha = 31$.

E	0.5	1	2	3	4	5
q= 7	sin	sin	sin	sin	PDB	PDB
q = 11	sin	sin	sin	sin	PDB	PDB

Time-domain simulations are performed using the Matlab programs which are similar to the EMTP simulation.[14] For cases including arresters, it can be seen that ferroresonant drop out will occur. Voltage and flux waveforms when MOA does not exist in the circuit at $V_{\rm in} = 3.1$ pu are shown in Figs. 8 and 9. Phase plane diagram is shown in Fig. 10. These figures show at $V_{\rm in} = 3.1$ pu, chaos occurs in the voltage transformer. When MOA exists in the circuit $V_{\rm in} = 3.1$ pu, behavior of system is periodic and chaotic oscillations change into periodic orbits and system becomes stable. Also at $V_{\rm in} = 6.3$ pu,

when MOA exists in the circuit chaos does not occur in the system and harmonic behavior appears in the terminal of voltage transformer.

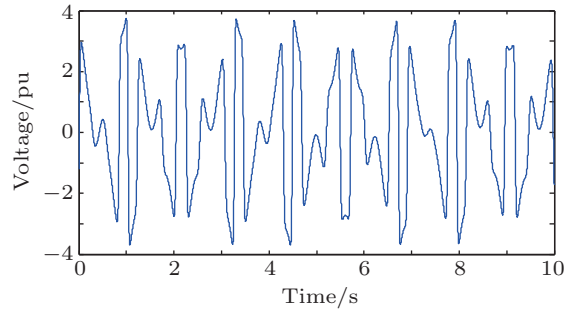


Fig. 8. (color online) Voltage waveform without MOA at $V_{\text{in}} = 3.1$ pu.

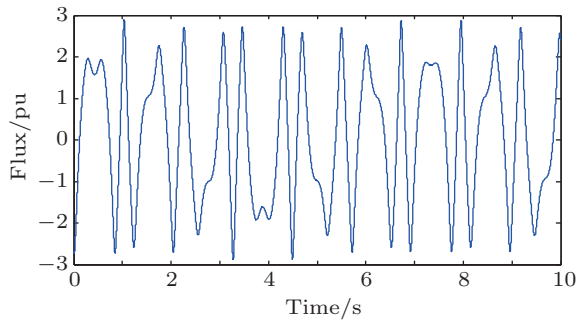


Fig. 9. (color online) Flux waveform without MOA at $V_{\text{in}} = 3.1$ pu.

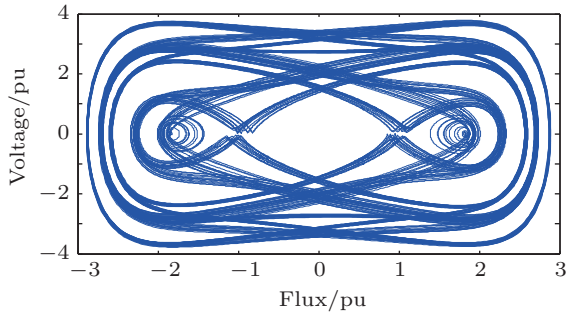


Fig. 10. (color online) Phase plane diagram without MOA at $V_{\text{in}} = 3.1$ pu.

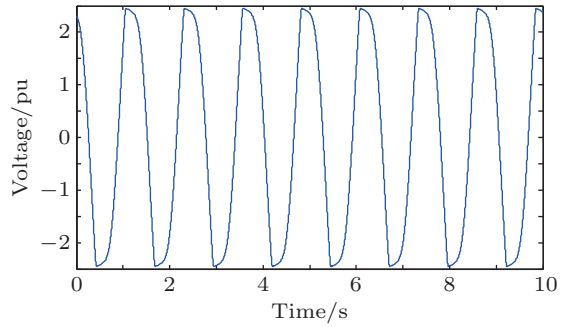


Fig. 11. (color online) Voltage waveform with MOA at $V_{\text{in}} = 3.1$ pu.

Figures 11–16 show that chaotic region mitigates by applying MOA surge arrester. The system shows a greater tendency for chaos for saturation characteristics with lower knee points, which corresponds to higher values of exponent q.

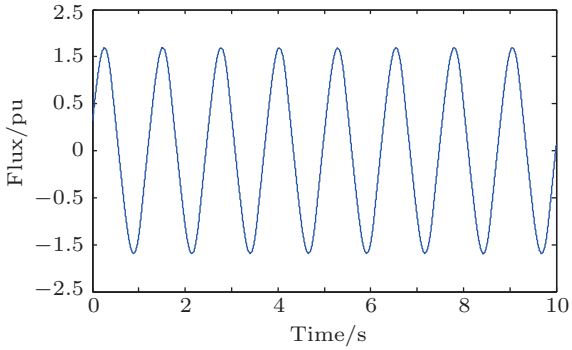


Fig. 12. (color online) Flux waveform with MOA at $V_{\text{in}} = 3.1$ pu.

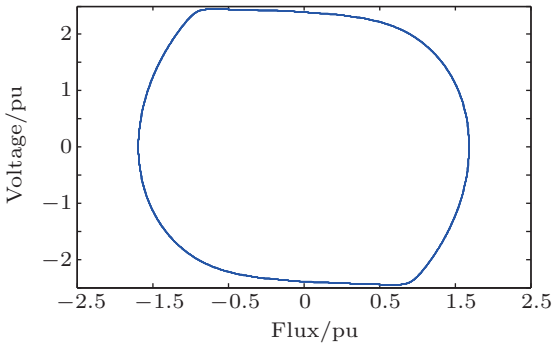


Fig. 13. (color online) Phase plane diagram with MOA at $V_{\text{in}} = 3.1$ pu.

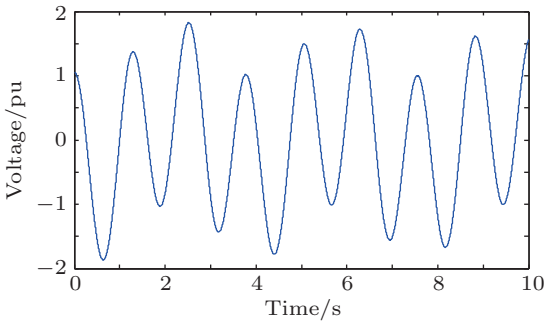


Fig. 14. (color online) Voltage waveform with MOA at $V_{\text{in}} = 6.3$ pu.

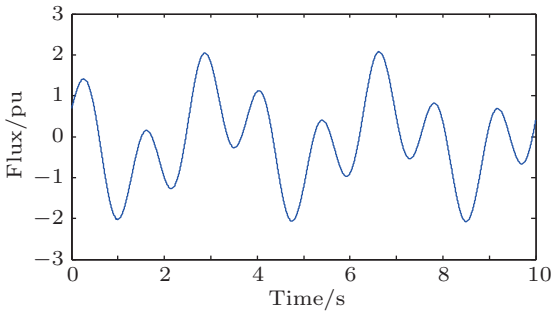


Fig. 15. (color online) Flux waveform with MOA at $V_{\text{in}} = 6.3$ pu.

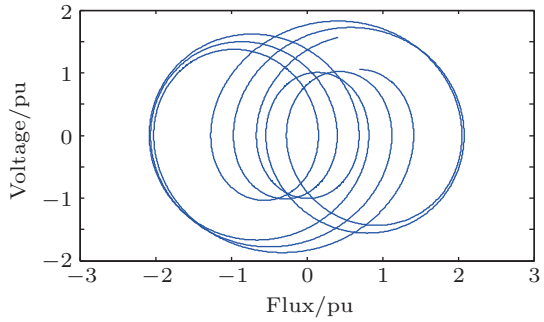


Fig. 16. (color online) Phase plane diagram with MOA at $V_{\rm in} = 6.3$ pu.

Considering Fig. 17, MOA makes a mitigation in chaotic behavior in the voltage transformer. The chaotic regions are removed and the behavior of system is periodic. At $q = 7$ and 11, MOA eliminates chaotic oscillations in the voltage transformer. Tendency to chaos exhibited by the system increases while q increases too. Bifurcation diagrams when MOA exists in the circuit for $q = 7$, 11 are shown in Fig. 17. For these two cases, α is 25. These figures prove that when q is increased, complexity of behavior of system increases, and that the behavior of system at $q = 7$ is more stable than $q = 11$.

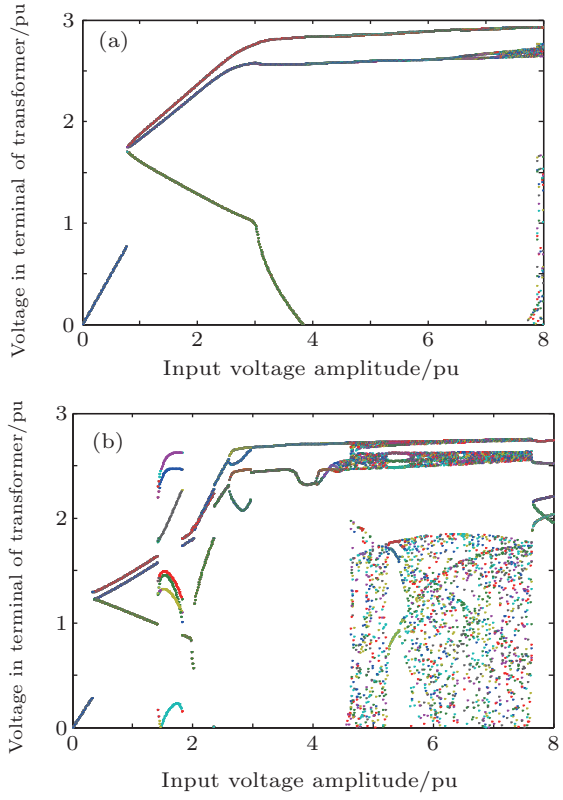


Fig. 17. (color online) Bifurcation diagram with MOA at (a) $\alpha = 25$ and $q = 7$; (b) $\alpha = 25$ and $q = 11$. Also bifurcation diagrams when $\alpha = 31$ are shown in Fig. 18. By increasing α chaotic regions are eliminated and for the high value of $V_{\rm in}$ behavior of system remains periodic.

Bifurcation diagrams for case that $C_{\rm ser}$ is considered as bifurcation parameter are shown in Fig. 19. These figures prove that by decreasing q ferroresonance oscillations can be removed and behavior of system can be stabilized too.

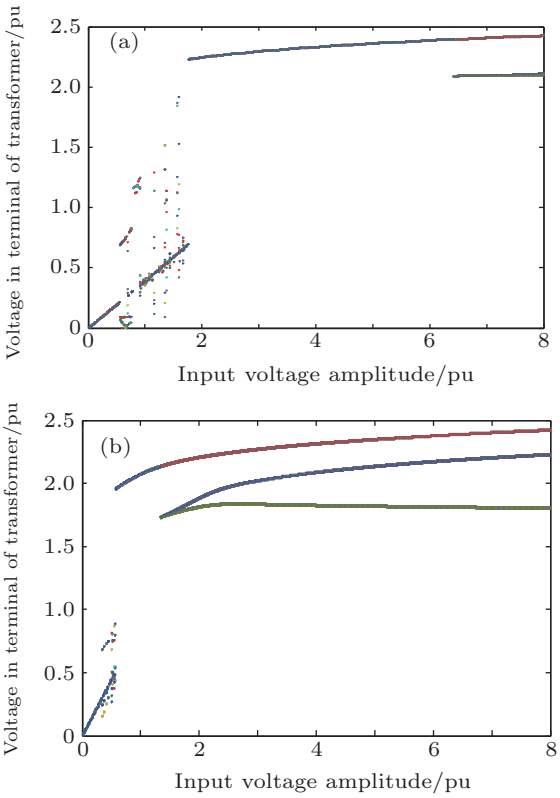


Fig. 18. (color online) Bifurcation diagram with MOA at (a) $\alpha = 31$ and $q = 7$; (b) $\alpha = 31$ and $q = 11$.

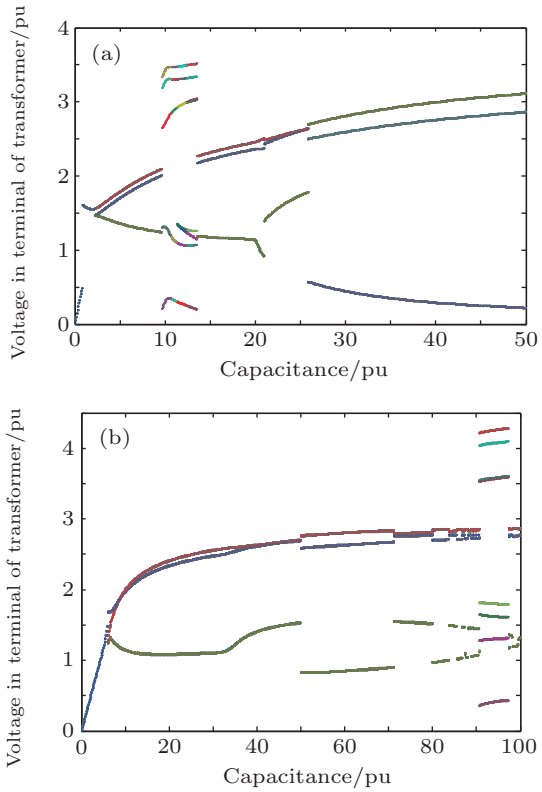


Fig. 19. (color online) Bifurcation diagram with MOA at (a) $\alpha = 25$ and $q = 11$; (b) $\alpha = 25$ and $q = 7$.

6. Conclusion

In this paper, the chaotic ferroresonant oscillations of the voltage transformer considering nonlinear model of core loss

and MOA were investigated. The presence of the MOA results in clamping the ferroresonant overvoltages in the studied system. The MOA successfully suppresses or eliminates the chaotic behaviour of proposed model. Consequently, the system shows less sensitivity to initial conditions in the presence of the arrester. It is seen from the bifurcation diagram that chaotic ferroresonant behavior depends on parameter q and α. MOA makes mitigation in ferroresonance chaotic behavior in the voltage transformer that in down value of q the chaotic region are removed and the behavior will be periodic. System stability increased with decreasing q and chaotic regions are eliminated. It is found when $q = 11$ at V_{in}= 4 pu, behavior of system is chaotic while for $q = 7$ in the same value of vin system is in harmonic mode and its stability is more than case that $q = 11$. By increasing α chaotic regions are eliminated and for the high value of vin behavior of system remains periodic. The bifurcation and chaos were analyzed and different types of bifurcation were obtained by using the multiple scales method. Also, Lyapunov exponents were calculated for different fixed points of bifurcation diagrams. It was shown that the chaos can occur in the voltage transformer in the form of PDB sequence. It was shown that the nonlinear model of core loss causes a delay in chaotic ferroresonant oscillations. The presence of nonlinear terms in core loss function causes more regular PDBs. Period-n windows with $n = 1, 2, 4, 8$ were observed in the phase plane diagrams. The periodic and aperiodic solutions and also the type of bifurcation were obtained for fixed points. PDB, SNB, HB and chaos were some of these bifurcations. Border collision bifurcation was detected in the ferroresonant behavior and occurrence reasons of this bifurcation were explained. The Feigenbaum number and eigenvalues were calculated for the stability analysis. The Feigenbaum number shows the accuracy of PDB sequence.

References

[1] Milicevic K and Emin Z 2011 *Int. J. Circ. Theory Appl.* **41** 259
[2] Forsen A and Kristiansson L 1974 *Int. J. Circ. Theory Appl.* **2** 13
[3] Hui M, Zhang Y B and Liu C X 2008 *Chin. Phys. B* **17** 3258
[4] Charalambous C A, Sturgess J P and Wang Z D 2011 *IET Gener. Transm. Dis.* **5** 640
[5] Nikolaidis V C, Milis I and Rizopoulos G 2012 *IEEE Trans. Power Del* **27** 300
[6] Sakarung P and Chatratana S 2005 *International Conference on Power Systems Transients,* June 2005 Canada, p. 19
[7] Kavasseri R G 2006 *Elect. Power Energy Syst.* **28** 207
[8] Escudero M V, Dudurych I and Redfern M A 2007 *Elect. Power Energy Syst.* **77** 1506
[9] Wornle F, Harrison D K and Zhou C 2005 *IEEE Trans. Power Del.* **20** 191
[10] Emin Z, Al-Zahawi B A T, Tong Y K and Ugur M 2001 *IEEE Trans. Circ. Syst. I* **48** 757
[11] Rezaei-Zare A, Sanaye-Pasand M, Mohseni H, Farhangi Sh and Iravani R 2007 *IEEE Trans. Power Del.* **22** 919
[12] Ben-Tal A, Shein D and Zissu S 1999 *Elect. Power Syst. Res.* **49** 175
[13] Moses P S, Masoum M A S and Toliyat H A 2011 *IEEE Trans. Energy Conversion* **26** 581
[14] Mozaffari S, Sameti M and Soudack A C 1997 *IEE Proc. Gen. Trans. Dist.* **144** 456
[15] Kuznetsov Y A 1998 *Elements of Applied Bifurcation Theory* (2nd edn.) (New York: Springer Verlag) pp. 1–115
[16] Abbasi H R, Gholami A, Rostami M and Abbasi A 2011 *Iranian Journal of Electrical & Electronic Engineering* **7** 42
[17] Kousaka T, Ueta T, Ma Y and Kawakami H 2005 *Int. J. Circ. Theory Appl.* **33** 263
[18] Tse C K 1994 *Int. J. Circ. Theory Appl.* **22** 263
[19] He S B, Sun K H and Zhu C X 2013 *Chin. Phys. B* **22** 050506
[20] Zhang X D, Liu X D, Zheng Y and Liu C 2013 *Chin. Phys. B* **22** 030509
[21] Chakravarthy S K and Nayar C V 1995 *Elect. Power Energy Syst.* **17** 267
[22] Abbasi A, Radmanesh H, Rostami M and Abbasi H 2009 *IEEE Conference of EEEIC09*, November 2009 Wroclaw, Poland, p. 97
[23] Abbasi A, Rostami M, Radmanesh H and Abbasi H R 2009 *IEEE Conference of EEEIC09,* November 2009 Wroclaw, Poland, p. 76
[24] Al Anbari K, Ramanjam R, Keerthiga T and Kuppusamy K 2001 *IEE Proc. Gen. Trans. Dist.* **148** 562
[25] Al Anbarri K, Ramanujam R, Saravanaselvan R and Kuppusamy K 2003 *Elect. Power System Res.* **65** 1
[26] Hui M and Liu C X 2010 *Chin. Phys. B* **19** 120509
[27] Pattanapakdee K and Banmongkol C 2007 *International Conference on Power Systems Transients (IPST)*, June 2007 France, p. 151
[28] Abbasi A, Rostami M, Fathi S H, Abbasi H R and Abdollahi H 2010 *Energy Power. Eng.* **2** 254
[29] Escudero M V, Dudurych I and Redfern M A 2007 *Elect. Power Syst. Res.* **77** 1506
[30] Li N, Yuan H Q, Sun H Y and Zhang Q L 2013 *Chin. Phys. B* **22** 030508
[31] Ben-Tal A, Kirk V and Wake G 2001 *IEEE Trans. Power Del.* **16** 105
[32] Zhang R X and Yang S P 2010 *Chin. Phys. B* **19** 020510
[33] Nayfeh A H 2004 *Applied Nonlinear Dynamics Analytical, Computational and Experimental Methods* (WILEY-VCH Verlag GmbH & Co. KGaA) pp. 1–225
[34] Hui M, ZhangY B and Liu C X 2009 *Chin. Phys. B* **18** 1787
[35] Tse C K 2003 *Complex Behavior of Switching Power Converters* (Boca Raton, USA: CRC Press) pp. 1–155
[36] Argyris J, Faust G and Haase M 1994 *An Exploration of Chaos* (New York: North-Holland)